Rectification of vortex motion in a circular ratchet channel

N. S. Lin, T. W. Heitmann, K. Yu, B. L. T. Plourde, and V. R. Misko

Phys. Rev. B **84**, 144511 — Published 7 October 2011

DOI: 10.1103/PhysRevB.84.144511

Rectification of Vortex Motion in a Circular Ratchet Channel

N. S. Lin[1], T. W. Heitmann[2], K. Yu[2], B. L. T. Plourde[2], and V. R. Misko[1]
[1]*Department of Physics, University of Antwerpen, Groenenborgerlaan 171, B-2020 Antwerpen, Belgium*
[2]*Department of Physics, Syracuse University, Syracuse, New York 13244-1130, USA*
(Dated: September 6, 2011)

We study the dynamics of vortices in an asymmetric (i.e., consisting of triangular cells) ring channel driven by an external ac current I in a Corbino setup. The asymmetric potential rectifies the motion of vortices and induces a net vortex flow without any unbiased external drive, i.e., the ratchet effect. We show that the net flow of vortices strongly depends on vortex density and frequency of the driving current. Depending on the density, we distinguish a "single-vortex" rectification regime (for low density, when each vortex is rectified individually) determined by the potential-energy landscape inside each cell of the channel (i.e., "hard" and "easy" directions) and "multi-vortex", or "collective", rectification (high density case) when the inter-vortex interaction becomes important. We analyze the average angular velocity ω of vortices as a function of I and study commensurability effects between the numbers of vortices and cells in the channel and the role of frequency of the applied ac current. We have shown that the commensurability effect results in a stepwise $\omega - I$ curve. Besides the "integer" steps, i.e., the large steps found in the single vortex case, we also found "fractional" steps corresponding to fractional ratios between the numbers of vortices and triangular cells. We have performed preliminary measurements on a device containing a single weak-pinning circular ratchet channel in a Corbino geometry and observed a substantial asymmetric vortex response.

PACS numbers: 74.25.Uv, 74.78.Na, 05.70.Ln

I. INTRODUCTION

A net flow of particles under unbiased external fluctuations/drive due to an asymmetric potential, which is called ratchet effect, has received much attention during the last decades. The transport and dynamical properties of particles on asymmetric potential have been widely studied, e.g., in physics and biology[1–8]. Random motion of particles can be rectified in such an asymmetric system, which can be used for, e.g., controlling particles motion, separating different types of particles (i.e., molecular sieves), for both underdamped and overdamped particles[4] and for molecular motors[5]. Vortices in a type II superconductor often (e.g., for magnetic field close to H_{c1}) can be treated as classical overdamped "particles". Most of the experiments on vortex motion rectification used arrays of asymmetric pinning sites (e.g., nanoengineered antidots or triangular magnetic dots/inpurties) to create an asymmetric potential, which rectifies the motion of vortices[8–14,27]. The rectified vortex motion was directly observed in experiments by imaging vortices via Lorentz microscopy[15]. Periodic arrangement of point defects of a gradual density or periodic square array of ferromagnetic dots of decreasing size, i.e., varying the density of pinning sites or the size of pinning sites, were shown to result in a ratchet potential[16,17]. When vortices are trapped by pinning sites, the repulsive vortex-vortex interaction creates a higher energy barrier near the area with higher density of pinning sites. Therefore, an asymmetric potential can be created by the gradient of the density of pinning sites[16]. Even without spatial asymmetry (i.e., without any asymmetric walls/boundaries or asymmetric pinning sites), the motion of vortices still can be controlled by time-asymmetric driving force[18–20]. Due to the possibility of controlling their motion, the dynamical behavior of vortices in such systems has attracted considerable interest. A series of elastic and plastic vortex flow phases were found[21–23]. Besides the liquid-like and solid lattice phase, vortex motion also revealed a jamming behavior[23,24]. When the density of vortices is changed, the vortex flowing direction can change to the opposite[9,10,17,25], which means vortices can drift in either the "hard" direction or the "easy" direction of the ratchet, depending on the vortex density. By controlling the motion of vortices, it is possible to remove vortices or reduce the vortex density by using a combination of two opposite oriented ratchet arrays[26]. The order of vortices and commensurability between vortices and cells also play an important role in vortex dynamics[17,23,25,27]. In two-dimensional (2D) ratchets, a transverse rectification was first predicted theoretically in Ref.[28] and then further studied in theory[4,29] and in experiments[30,31].

In the present paper, we study the dynamics of vortices in a circular channel formed by asymmetric triangular (funnel) cells (TCs) (see Fig. 1) [note that earlier this approach to form asymmetric channels in experiment (i.e., using weak-pinning channels) was employed in a stripe geometry[6]]. Due to the radially flowing current in a Corbino setup[33–40], the driving force is not uniform inside the cell which is different from linear ratchet channels. Such a geometry (i.e., asymmetric in the azimuthal direction and in the radial direction), as will be shown, leads to a specific dynamical behavior, for example, a vortex located near the inner corner of a TC (which is closer to the center), experiences a stronger driving force and moves to the next TC while a vortex located near the outer corner

of TC does not move. The circular geometry of the ratchet channel is convenient for studying commensurability and step-motor (phase locking) behavior[13,23]. We analyze in detail low and high density regimes of rectification, i.e., "single-vortex" and "multi-vortex" regimes. We demonstrate that the mechanism of rectification are qualitatively different for these two cases. In addition, we have performed preliminary measurements using a single nanofabricated weak-pinning ratchet channel of a-NbGe with strong-pinning NbN channel edges in a Corbino set-up, and we observed a substantial asymmetric vortex response.

This paper is organized as follows. First in Sec. II, the model of our systems will be presented. Then in Sec. III, we will show how the density of vortices and the frequency of driving current influences the dynamical behavior of vortices. Commensurability effects of vortex density and of the frequency of current will be discussed in Sec. IV. We present the measurements of a vortex ratchet in a Corbino geometry in Sec. V. Finally, the conclusions will be given in Sec. VI.

II. MODEL AND SIMULATION

We consider a ring-like weak-pinning channel constructed of N partially overlapping TCs as shown in Fig. 1. In our simulations, the radius of the ring R is typically set as 6λ, where λ is the magnetic field penetration depth, the wider part of the channel (i.e., the base of TCs) $w = 0.75\lambda$, and the width of the narrow part Δ (the neck) is typically 0.1 of the wider part (i.e., the ratio $g = \Delta/w = 0.1$). We also performed simulations in a channel with a wider neck part, e.g., $g = 0.15$, for comparison. The weak-pinning channel (where vortices can move freely) is surrounded by a strong-pinning superconducting material[32] which is modeled by a medium where vortices cannot move. An external current I radially flows from the center of the disk to the edge, resulting in the density of current $J(\rho) \sim I/\rho$. Therefore, the closer a vortex to the center of the disk, the stronger the Lorentz force that acts on it. The driving force due to the radial current is[33–38]

$$\boldsymbol{f}_i^d = \frac{\Phi_0 I}{2\pi\rho_i d}\,\hat{\theta} = \frac{f_0 I_0}{\rho_i}\,\hat{\theta}, \tag{1}$$

where $\hat{\theta}$ is the unit vector in the azimuthal direction in the disk plane, $f_0 = \Phi_0^2/(2\pi\mu_0\lambda^3)$ is the unit of force, $I_0 = \mu_0\lambda^2 I/(\Phi_0 d)$ is the dimensionless driving current, and Φ_0 is the flux quantum. We perform Langevin-type molecular dynamics (MD) simulations and numerically integrate the overdamped equations of motion[37,38,41,42]:

$$\eta\frac{d\boldsymbol{r}_i}{dt} = \boldsymbol{f}_i \tag{2}$$

with

$$\boldsymbol{f}_i = \sum_j \boldsymbol{f}_{ij}^{vv} + \boldsymbol{f}_i^T + \boldsymbol{f}_i^d + \boldsymbol{f}_i^b, \tag{3}$$

where η is the dimensionless viscosity coefficient which is set here to unity (note that the viscosity coefficient varies in different superconductors, e.g., in a-NbGe $\eta \approx 10^{-8}$ Ns/m^2[43]. Using this value of η in our calculations results in typical maximum values of vortex linear velocity $v \approx 10^2$ m/s (for a 1μm-thick film) which is still below the Larkin-Ovchinnikov critical velocity[44,45]).

The vortex interaction $\boldsymbol{f}_{ij}^{vv}$ is described by a first order of the modified Bessel function of the second kind $K_1(r_{ij}/\lambda)$, and the thermal force obeys

$$\langle \boldsymbol{f}_i^T(t)\rangle = 0, \tag{4}$$

and

$$\langle \boldsymbol{f}_i^T(t)\boldsymbol{f}_j^T(t')\rangle = 2\eta k_B T\delta_{ij}\delta(t-t'). \tag{5}$$

To model the vortex-boundary interaction, we assume an infinite potential wall at the boundary (i.e., vortices cannot leave the channel) which decays inside the triangular cell with the same dependence on position as the vortex-vortex interaction potential. The total interaction of a vortex with the channel boundaries is calculated by integrating the vortex-wall interaction potential over the geometrical boundary of the channel. The resulting potential due to the boundary is shown in Fig. 2, and the vortex-boundary force $\boldsymbol{f}_i^b$ is directly calculated from the potential.

In our simulations, we first set $T > 0$, when no current is applied, and then gradually decrease temperature to let the system to relax to the ground state. Then we set $T = 0$ and apply an external driving, i.e., an ac current resulting in oscillating Lorentz force with frequency ν and amplitude I_0 that acts on vortices, to study the dynamics of the system.

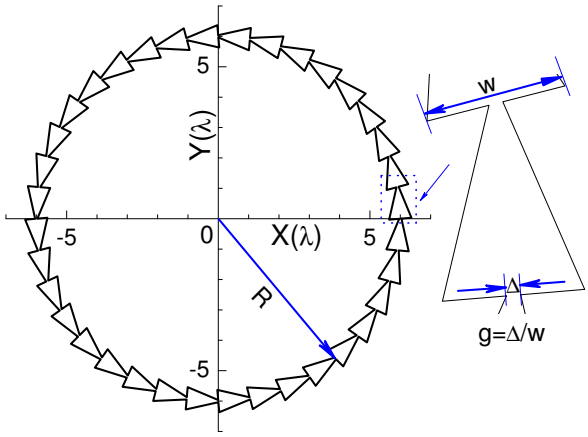

FIG. 1: (Color online) The geometry of the system. The widths of the wide part ω and narrow part Δ are shown in the figure, where $g = \Delta/w$ is the ratio between the two parts. Here $g = 0.1$, the radius of the channel $R = 6\lambda$ and the channel is constructed by 36 TCs, i.e., $N = 36$.

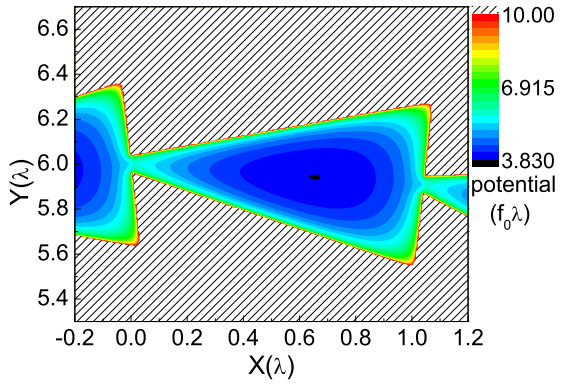

FIG. 2: (Color online) The contour map of the modeled potential. The lowest potential in a TC is close to the geometry center of the triangle and the potential near the boundary is high enough to prevent vortices from escaping the TC.

III. RECTIFICATION OF VORTEX MOTION

A. Density of vortices

The vortex density, i.e., the number of vortices per TC, plays an important role in the dynamics of the system. For very low vortex density, the vortex-vortex interaction is small as compared to the interaction with the boundary, and therefore it can be neglected. With increasing the vortex density, the interaction between vortices becomes important. Therefore, we roughly distinguish two regimes, i.e., a single-vortex regime and a multi-vortex regime, respectively, corresponding to low and high vortex density.

In order to characterize the dynamical behavior of the system of vortices, we calculate the net angular velocity (normalized on the number of vortices L) of each vortex and take average over all the vortices for, e.g., 100 ac periods. The resulting average angular velocity (called further "angular velocity") is denoted as ω which is analyzed for different parameters of the system and drivings. Note that angular velocity is related in a straightforward way to the flux-flow voltage[32,33] which can be measured in experiment.

One system contains L vortices and N triangles in a circular chain, e.g., in our simulations we take $N = 36$. If there is less than one vortex per cell, i.e., $L < 36$ in our system (see Fig. 1), then the density of vortices is low enough and one can neglect the interaction between vortices. One can imagine that all the vortices are far away from each

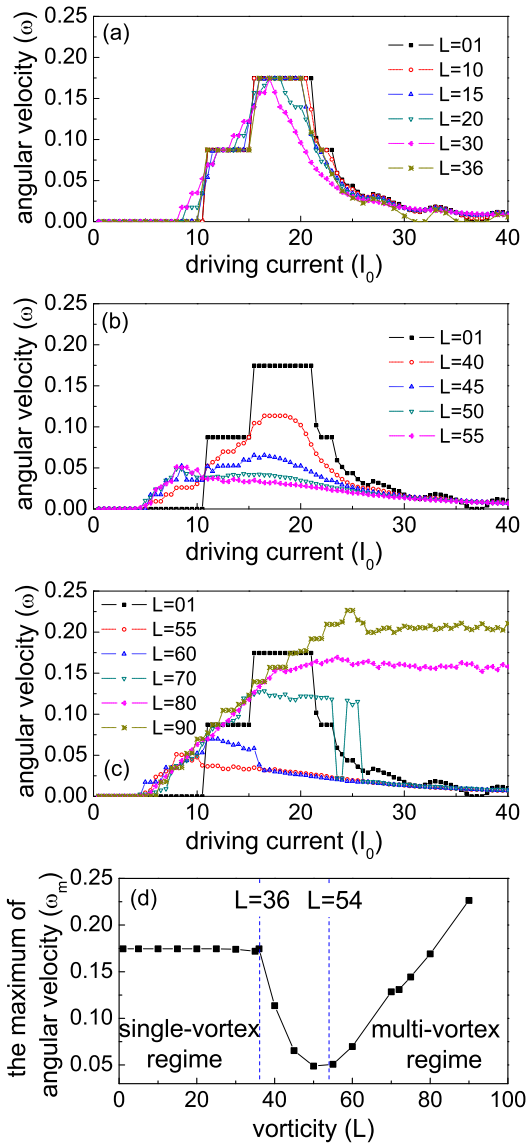

FIG. 3: (Color online) The $\omega - I_0$ curves for different density of vortices: (a) the density of vortices is low, $L = 1 - 36$ (in the single-vortex regime), the angular velocity reaches the same maximum; (b) the density increases, $L = 40 - 55$, the maximum of the angular velocity decreases; (c) for further increasing density, i.e., high density of vortices, $L = 55 - 90$, the maximum starts to increase and the critical value of the driving current, when the angular velocity starts decreasing, becomes larger; (d) the maximum of the angular velocity ω_m first remains the same until the number of vortices $L > 36$. Then the maximum ω_m first decreases, but for $L > 55$ it starts to increase.

other and weakly interact with other vortices but they are strongly influenced by the ratchet potential induced by the boundary. Therefore, the dynamical behavior in the low density case is similar to that of the system with just one vortex [shown in Fig. 3 (a)], which is considered in the single-vortex regime. Thus, for $L = 1 - 36$, the maximum of the angular velocity is the same value [see Fig. 3 (a)]. When the density increases and therefore the interaction

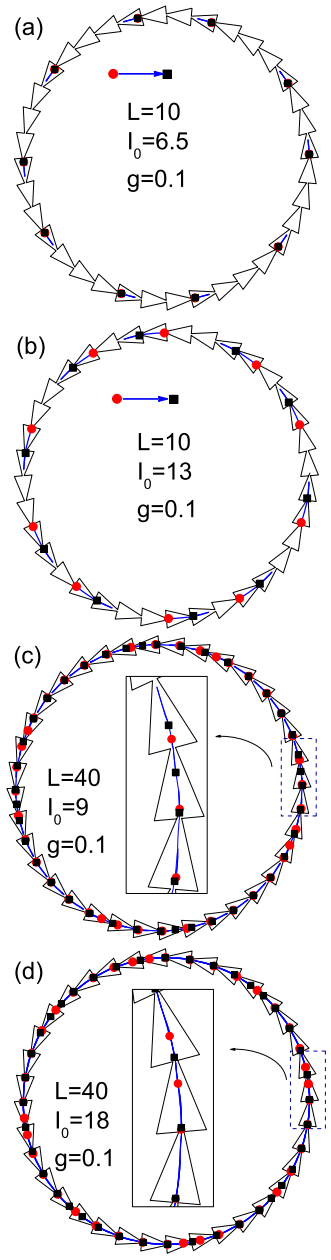

FIG. 4: (Color online) Trajectories of vortex motion, in the case of the low density of vortices ($L = 10$) (a), (b), and in the intermediate case ($L = 40$) (c), (d), for different values of driving current: $I_0 = 6.5$ (a), 13 (b), 9 (c), and 18 (d). The initial positions of the vortices are marked by gray circles and the final positions after one period of ac current are marked by black squares. The trajectories of vortices, which are plotted by solid lines, are nearly circular no matter that the current is large or small.

between the vortices becomes appreciable, the maximum of the angular velocity ω_m first decreases to 0.05 for $L = 55$ [see Fig. 3 (b)] and then starts to increase [see Fig. 3 (c)] when the system turns to the regime of high vortex density.

To understand this non-monotonic behavior of the maximum of the angular velocity ω_m [shown in Fig. 3(d)], we studied the trajectories of moving vortices. When the system is in the single-vortex regime, where $L \leq 36$, all the vortices move along a nearly circular trajectory no matter whether the applied current is small or large, which can be considered as a one-dimensional (1D) motion (shown in Fig. 4). For low driving currents, each vortex oscillates near its initial position inside a TC [e.g., see Fig. 4 (a)], and when the driving force reaches some critical value, all the vortices move with a net angular velocity ω in the easy direction [e.g., see Fig. 4 (b)]. However, in the multi-vortex regime, i.e., the high density case (e.g., $L = 80$), the motion of vortices is not 1D any more. The ac current drives vortices to pass through the narrow part (i.e., neck) of the channel in the easy direction and when current is alternated, some of vortices are forced to move into the corner by the others and "freeze" thus blocking the motion in the hard direction [shown in Fig. 5]. Due to the asymmetry in the radial direction and radially decreasing current density in the Corbino setup, a vortex near the inner corner, which is closer to the center of the disk, moves faster than the one near the outer corner. Therefore, at a specific value of the current [e.g., at $I_0 = 9$, as shown in Fig. 5(a)], the vortex near the inner corner has a larger angular velocity. When the current increases, more and more vortices move along the circular trajectory and the distribution of vortices becomes strongly inhomogeneous [shown in Fig. 5(b)]. With further increasing current, this 2D trajectory becomes narrow and all the vortices move along the circle, i.e., the 2D motion becomes 1D [shown in Fig. 5(c)]. With increasing density, more and more vortices remain in the area near the corners of TCs and block other vortices moving in the hard direction. Therefore, the maximum of vortex angular velocity increases. Even in the descending-velocity region of the single-vortex regime [see e.g., when $I_0 > 21$ in Fig. 3(c)], the angular velocity is still large.

The maximum of the angular velocity ω_m for different vorticities L is shown in Fig. 3(d). In the single-vortex regime (i.e., for not more than one vortex per TC, when the intervortex interaction is negligible), ω_m remains almost the same, $\omega_m = 2\pi/36 \approx 0.175$, i.e., in a single cycle each vortex moves over one TC. When L becomes larger, there are more than one vortex per TC and the repulsive vortex-vortex interaction in the same TC makes the 1D motion in either easy or hard directions much easier, due to incommensurability (see, e.g., Refs.[21,22]). Therefore, ω_m first decreases when $L > 36$. However, for $L \geq 55$, the maximum ω_m starts to increase. The reason for this behavior is the transition from 1D motion to 2D motion. When vortices move along 2D trajectories (see Fig. 3), the repulsive interaction between vortices still "helps" a vortex to move to the next TC in the easy direction but blocks the vortex motion in the hard direction until applying a large enough driving current. Our estimates show that for even larger L, i.e., for $L \gtrsim 120$, the maximum of the angular velocity ω_m starts to decrease. This is explained by the fact that for high vortex densities, vortex configurations inside the TCs become more rigid which prevents vortex motion in either direction and thus leads to the suppression of rectification. However, in this analysis we restrict ourselves to relatively moderate vortex densities when the London approximation is still valid.

The radial asymmetry facilitates the motion of vortices from inner/outer corners (driven by stronger/weaker force) one by one. This is different from the case of a linear ratchet channel where two vortices in the corners are driven by the same force and, as a result, arrive simultaneously at the neck region leading to jamming. In an asymmetric channel, the symmetry is broken, and jamming occurs only for rather large driving force.

B. Frequency dependence

The dynamical behavior of vortices in the considered ratchet system is also strongly influenced by frequency of the ac current. In this subsection we study frequency dependence of the rectified vortex motion. For different frequencies ν, the $\omega - I_0$ curves are shown in Fig. 6.

When the frequency is low, the dynamical behavior is similar for different vortex densities. As the drive amplitude I_0 is increased, the angular velocity first increases, reaches a maximum, and then decreases to zero. The curves, especially for $L = 1$, in Fig. 6(a) are similar to the analytic result in a ratchet potential (e.g., see Fig. 2 in Ref.[26]). In the case of $L = 1$, the first critical value of current I_{c1} [shown in Fig. 6(a)] corresponds to the maximum friction in the easy direction f_m^+ and the second one I_{c2} corresponds to the case when the driving force reaches the maximum friction in the hard direction f_m^-. When $L = 40$, the first critical value of current decreases to I'_{c1}, which means vortices are easier to move in the easy direction. If the density increases further, I'_{c1} decreases and I'_{c2} increases, for $L = 80$ [shown in Fig. 6(a)]. Therefore, the interaction between vortices allows vortices to move even easier in the easy direction and harder in the hard direction.

For an intermediate frequency [e.g., $\nu = 1$ as shown in Fig. 6(c)], when the distance a vortex moves during one period is comparable to the size of a TC, the dynamical behavior of vortices will depend not only on the driving force but also on the vortex density. This is explained by the fact that the confinement force due to the boundary and the vortex-vortex interaction are also comparable. In this case we obtain different dynamical behavior in single-vortex

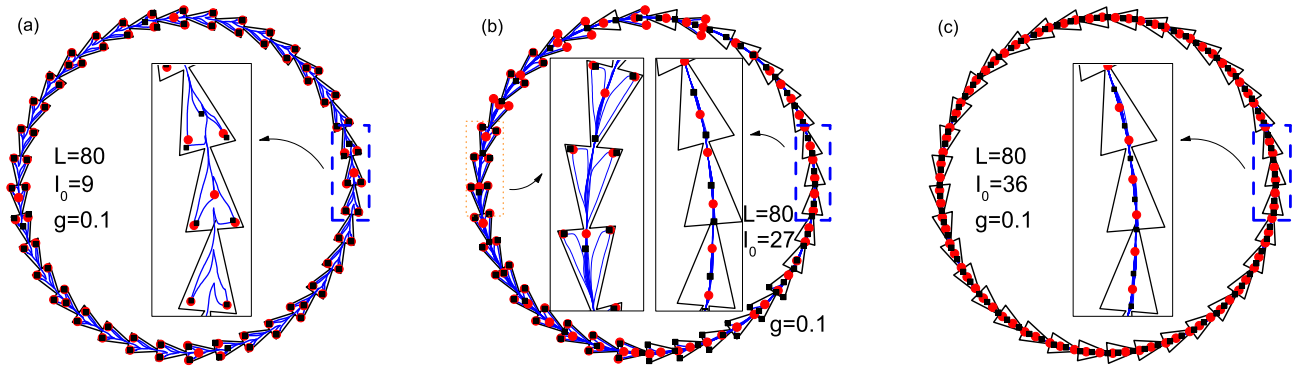

FIG. 5: (Color online) Trajectories of vortex motion during one ac period in the case of high density of vortices ($L = 80$), i.e., the multi-vortex regime, for different values of the driving current, $I_0 = 9$ (a), 27 (b), and 36 (c). When the current is in a certain range $I_0 = 5 - 19$ [see Fig. 3 (c)], the vortices move along 2D trajectory [e.g., $I_0 = 9$, shown in (a)] which is different from the circular 1D trajectories in the low density case. With increasing current, more vortices start to move along circular trajectories and thus 2D trajectories finally turns to a 1D circle [e.g., see (c)]. During the transition from the 2D to 1D motion, the distribution of vortices becomes inhomogeneous [shown in (b)].

and multi-vortex regimes which were discussed in the previous subsection. Due to the commensurability between the numbers of TCs and vortices, a step structure of the $\omega - I_0$ curve is revealed in the low density case (e.g., $L = 1$ and $L = 10$), which will be discussed in more detail in Sec. IV.

As one can predict, the angular velocity becomes zero [see Fig. 6(e)] when the frequency is high enough because a vortex oscillates near its initial position inside a cell and thus its motion cannot be rectified. Therefore, the variation of the angular velocity is much smaller than that in the low/intermediate frequency case. Each vortex is localized in a specific TC, i.e., the vortex is only influenced by a single potential well but not by the ratchet potential.

For comparison, we also calculate $\omega - I_0$ curves for the case when a TC has a wider connection part ($g = 0.15$) [shown in Fig. 6(b), (d), (f)]. The function $\omega(I_0)$ in general shows a similar behavior as for $g = 0.1$. However, for the intermediate frequency ($\nu = 1$) of the applied current, we obtain more steps in $\omega - I_0$ curve in the case of $L = 1$ [shown in Fig. 6(d)] than that for $g = 0.1$ [shown in Fig. 6(c)]. This relates to the commensurability effect that will also be discussed in Sec. IV.

IV. COMMENSURABILITY EFFECT

A. Commensurability of vortex density

As we defined above, the system contains L vortices and N triangles in a circular chain. If there is a common integer (except one) in terms of which two numbers L and N can both be measured, then they are commensurate. Otherwise, they are incommensurate. Fig. 7 shows the average angular velocity ω as a function of I_0 for different commensurate ratios. The ascending part of the $\omega(I_0)$ curves (i.e., where ω versus I_0 increases) is stepwise. Besides the large steps of angular velocity in the $\omega - I_0$ curve for $L = 1$, which we refer to as "integer steps", we also found smaller steps for some specific vorticities L (shown in Fig. 7). If $L/N = k/m$ and $k \neq 1$, where k and m are incommensurate integers, the small steps can be found in the $\omega - I_0$ curves [in Fig. 7(b)-(d)]. Note that these steps can also be observed in the descending part of the $\omega(I_0)$ curves, although they are less pronounced [i.e., for $L = 1$ in Fig. 7], and for large drivings (and small ω) these "steps" can be seen as oscillations in $\omega(I_0)$. The origin of these steps, as well as those in the descending part of the function $\omega(I_0)$, is explained by commensurability effects between the vortex-traveling distance and the size of the TC. However, for large drivings a vortex travels an additional "loop" without being rectified.

When $k = 1$, we observe only integer steps of the angular velocity $\omega(I_0)$ [in Fig. 7(a)]. The difference in the angular velocity between two adjacent steps is always ω_0. If $k \neq 1$, then we can find a fractional step whose magnitude is ω_0/k. For example, for $k = 2$ [shown in Fig. 7(b)], the smallest step is $\omega_0/2$ in the system with 72 vortices (i.e., $L = 72$), which is a half of that for $k = 1$ (e.g., when $L = 36$). In the case of $k = 1$, a unit cell contains only one vortex. [The "unit cell" (UC) is a minimum repeatable set of TC(s) containing an integer number of vortices. For example, for $L = 1$ the UC is the entire channel with one vortex, and for $L = 36$ the UC is one TC with one vortex.]

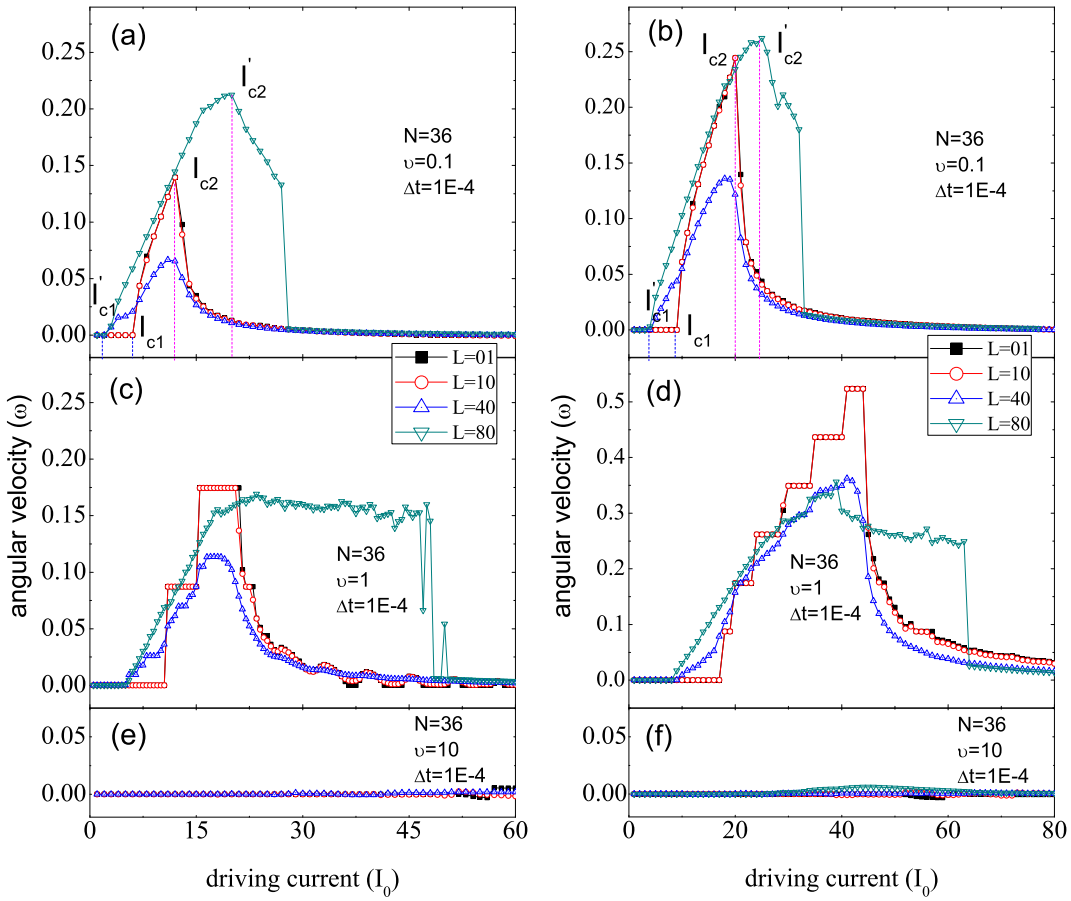

FIG. 6: (Color online) The $\omega - I_0$ curves for different frequencies: $\nu = 0.1$ (a), (b), $\nu = 1$ (c), (d), and $\nu = 10$ (e), (f). (a), (c), and (e) are in the system with a narrower neck, $g = 0.1$, and (b), (d), and (f) are in the system with a wider neck $g = 0.15$. The scale of ω in panel (d) is different from the others. For low frequency current (e.g., $\nu = 0.1$) the ratchet effect is clearly seen [as shown in (a) and (b)]. In this case, the angular velocity first increases continuously to the maximum and then decreases to zero. For intermediate frequency $\nu = 1$, besides the ratchet effect, the effect of commensurability, i.e., discontinuity in the angular velocity $\omega(I_0)$ (see Sec. IV), has a clear influence on the $\omega - I_0$ curve [e.g., see (c) and (d) for $L = 1$ or $L = 10$]. For high frequency current (e.g., $\nu = 10$), vortices are confined in their initial TCs and only oscillate in a single potential well. Therefore, the effect of the periodic ratchet potential disappears [shown in (e) and (f)].

If one vortex can overcome the potential barrier and move in the easy direction, all the vortices can do so at the same time, i.e., collectively. This results in integer steps of the average angular velocity ω_0 in the $\omega - I_0$ curve. However, fractional steps appear when there are more than one vortex in each UC. For instance, a UC contains one TC with two vortices when $L = 72$, and if $L = 24$, the UC is constructed by three TCs with two vortices. In general case, the unit cell contains m TCs with k vortices inside. If $k > 1$, there are more than one vortex in the UC, and those vortices are not equivalent, i.e., they are not located at the equivalent position in the TC and/or they experience different interactions with the boundary. Therefore, they move with different angular velocities in each period. Let us take $k = 2$, for example (see Fig. 8). As shown in Fig. 8(a), the vortices located in a TC that is followed by an empty TC in the easy direction (type-A) can overcome the potential barriers in a period of alternating current and move to its neighbor TC, while the others (type-B) are still localized in its original TC. When $I_0 = 10$ [shown in Fig. 8(b)], type-A vortices move from C2 to C3 but type-B vortices only oscillate in C1. In the view of the whole circular channel, only a half of vortices (i.e., type-A vortices) move to another TC while the other half of vortices (i.e., type-B vortices) do not move. After that, the type-B vortices are located at similar position as type-A vortices in the previous cycle, i.e., the previous type-B vortices now become type-A vortices and they will move to next TC in the anticlockwise direction during the next period. Therefore, when we calculate the average angular velocity for all the vortices, the value is a half of the angular velocity of type-A vortices, i.e., $\omega_0/2$. If the current increases, every vortex can overcome the barriers and move to the neighbor TC [e.g., as shown in Fig. 8, type-A vortices move from

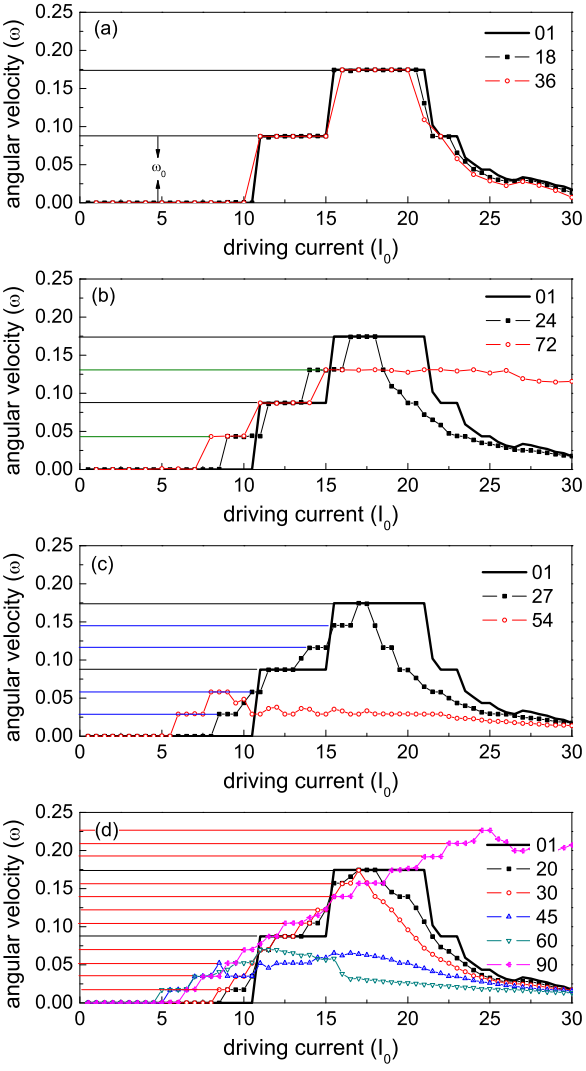

FIG. 7: (Color online) The $\omega - I_0$ curve for a channel with $g = 0.1$ and different k: $k = 1$ (a), 2 (b), 3 (c), and 5 (d). L is the vorticity, i.e., the number of vortices. N is the number of cells in the circular chain. If $L/N = 1/m$, e.g., $L = 1, 36$, the $\omega - I_0$ curve shows several steps and the height of each integer step is ω_0. When $L/N = k/m$ (k=2, 3, 5), the height of each fractional step is ω_0/k [e.g., as shown in (b) (c) and (d)].

C2 to C3 and type-B vortices move from C1 to C2 when $I_0 = 13$]. Then average angular velocity becomes ω_0 which is the same as that for $k = 1$ when all vortices move to the neighbor TC.

We also analyze the effect of the thermal fluctuations on rectification. For this purpose, we performed simulations for few non-zero values of temperature. When the temperature increases, the $\omega - I_0$ curves become smoother (see Fig. 9) since the effect of commensurability is suppressed by thermal fluctuations. Both the integer steps and fractional steps become smeared out due to the fluctuations. The ratchet effect becomes weaker with increasing temperature, e.g., for $L = 24$ at $T = 5 \times 10^{-3}$, as shown in Fig. 9(b). Note that the considered dimensionless values of temperature correspond to real temperatures below 1 K which are well below the superconducting transition temperature T_c of our weak-pinning channels.

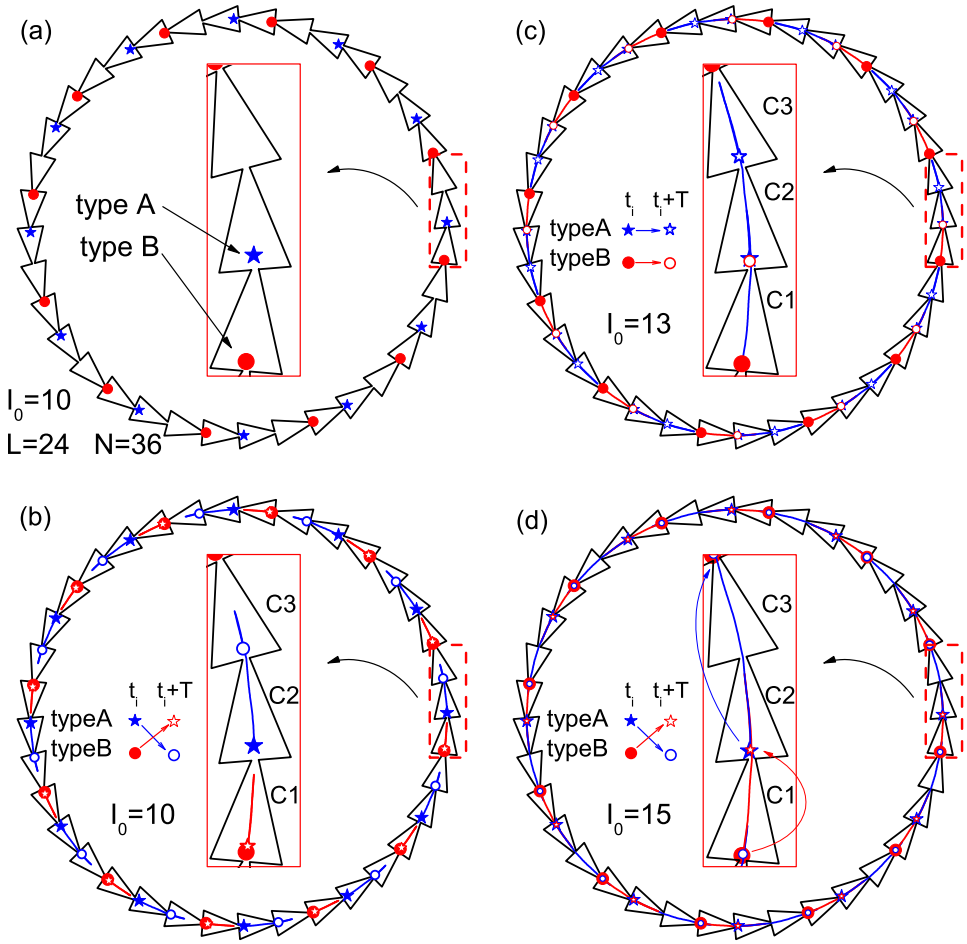

FIG. 8: (Color online) (a) The configuration of 24 vortices after 1000 periods of oscillations, $t = t_i$. The moving trajectories of vortices in one period of ac current, i.e., from $t = t_i$ to $t = t_i + T$, is shown for $I_0 = 10$ (b), 13 (c), and 15 (d). The insets of (a)-(d) show the vortex distribution in a unit cell. For $L = 24$, a type-A vortex is the vortex in a triangular cell (TC) [e.g., TC C2 in the inset of (a)] that has a neighbor empty TC in the easy direction [e.g., TC C3 in the inset of (a)], i.e., a TC without vortex, while a type-B vortex is in a TC [e.g., TC C1 in the inset of (a)] that neighbors a TC with type-A vortex inside. When the current drives vortices in the easy direction (e.g., $I_0 = 10$), two types of vortices move in different ways. Type-A vortices move from C2 to C3 but type-B vortices do not move to C2 due to a larger repulsive interaction in the easy direction (b). When $I_0 = 13$ (c), $\omega = \omega_0$ is the same as the integer step in $\omega - I_0$ curve [see Fig. 7(b)]. The type-A (type-B) vortex moves over one TC and remains type-A (type-B) in the end of the period. If the current increases further, e.g., $I_0 = 15$, type-A and type-B vortices move with different net angular velocities and after every period they switch their type [shown in (d)].

B. Commensurability effect of frequency

Further we analyze the angular velocity evolution while varying the ac drive frequency (shown in Fig. 10). For varying frequency ν, the $\omega - \nu$ curves are characterized by peaks and/or oscillations. Let us clarify this behavior. As discussed in Sec. III, if $f_m^- > f^d > f_m^+$, vortices can move in the easy direction and be frozen/blocked in the hard direction when the current alternates. Let us introduce a time scale, T_0, to characterize the motion of a vortex over the entire TC. One TC occupies an angle $\theta_0 = 2\pi/N$. If we assume that a vortex moves over the entire TC to the equivalent position in the next TC, then T_0 should satisfy the following condition:

$$\int_0^{T_0} \omega dt = \int_0^{T_0} [\boldsymbol{f}^d(I_0) + \boldsymbol{f}^b + \boldsymbol{f}^{vv}] \cdot \hat{\theta} dt/\eta r = \theta_0, \tag{6}$$

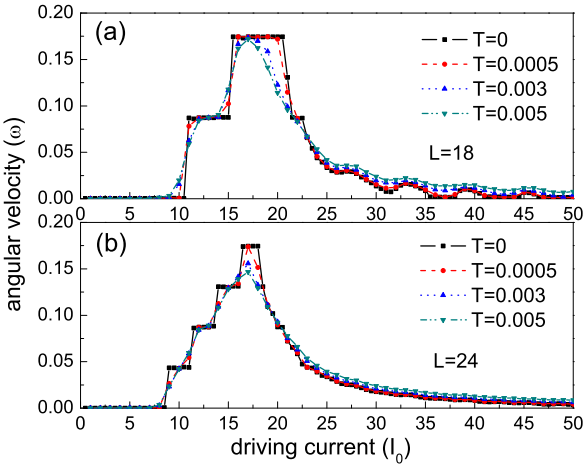

FIG. 9: (Color online) The effect of temperature fluctuations: the $\omega - I_0$ curves for different temperatures for (a) L=18 and (b) L=24. Both the integer and fractional steps are smeared out, i.e., the commensurability effect is reduced by increasing temperature. When large enough, the thermal fluctuations reduce the ratchet effect, e.g., for $L = 24$ and $T = 5 \times 10^{-3}$ (b).

where $\hat{\theta}$ is the unit vector in the azimuthal direction. In the single vortex case ($L = 1$), we set $\boldsymbol{f}^{vv} = 0$, and θ_0 is a constant. Considering the circular trajectory of the moving vortex, the integral of $\boldsymbol{f}^b$ is also a constant. Therefore, T_0 only depends on the current I_0 and we use the notation $T_0(I_0)$ instead of T_0 in order to show the dependence on the driving current.

If $f_m^- > f^d(I_0) > f_m^+$ and the ac period $t = 2T_0(I_0) = t_0(I_0)$, then the rectified signal will be maximum since all the vortices coherently move over the entire TC in the easy direction during the first half period and do not move backwards in the next half period. Then we can obtain the principal period $t_0(I_0) = 2T_0(I_0)$ for each value of the current and roughly estimate forces f_m^- and f_m^+ from the $\omega - \nu$ or $\omega - t$ curves [as shown in Fig. 10]. The maximum angular velocity ω_m for different current and vorticities L is shown in the insets of Fig. 10. For example, in the case of $L = 1$ [see Fig. 10(a)], the angular velocity is always zero when $I_0 \leq 8$ and becomes non-zero for $I_0 = 10$, i.e., the vortex starts to move in the easy direction. Therefore, $f^d(I_0 = 8) < f_m^+ < f^d(I_0 = 10)$. However, for $I_0 \geq 22$, the maximum angular velocity ω_m decreases as compared to the case for $I_0 = 20$, which means $f^d(I_0 = 20) < f_m^- < f^d(I_0 = 22)$. For $f^d(I_0) > f_m^-$ when driving current increases, vortices move backwards (i.e., the motion in the hard direction) therefore resulting in the decreasing net angular velocity. For example, when $I_0 = 22$ [shown in Fig. 10(a)], the maximum ω_m becomes smaller and the jumps in the $\omega - t$ curves become smoother, which means the effect of boundary becomes weaker under a strong driving force. Therefore, the angular velocity should be zero when the driving force goes to infinity. It explains why the angular velocity decreases and goes to zero when the driving current increases above some critical value.

For the single-vortex case, the frequency dependence of the first local maximum ω_m' in the $\omega - \nu$ curves versus the corresponding drive frequencies, $\nu_0 = 1/t_0$, is plotted in Fig. 11 which shows a linear behavior. When the density is increased up to one vortex per cell ($L/N \leq 1$), the $\omega - t$ curve is similar to the one for $L = 1$ for both incommensurate [e.g., see Fig. 10(b)] and commensurate cases [see Fig. 10(c)] because the interaction between vortices is weak. For a higher density, the (in-)commensurability effect becomes pronounced. The sharp jumps of the angular velocity are obtained only in the commensurate case [e.g., $L = 72$ shown in Fig. 10(e)] but not in the incommensurate case [e.g., $L = 80$ shown in Fig. 10(f)]. Comparing the high density cases with the low density cases, we can conclude that sharp jumps in $\omega - t$ curve, which are both found in single-vortex and multi-vortex regimes, are due to the effect of periodically repeated boundaries of the ratchet potential and the increasing local maximum of the angular velocity when t increases in the multi-vortex regime. This is different from the single-vortex regime, because of the strong interaction between vortices induced by the high vortex density. If the principal period (i.e., the time period for the first jump) is denoted by t_0, the others will be harmonics of t_0, kt_0 ($k = 2, 3, ...$).

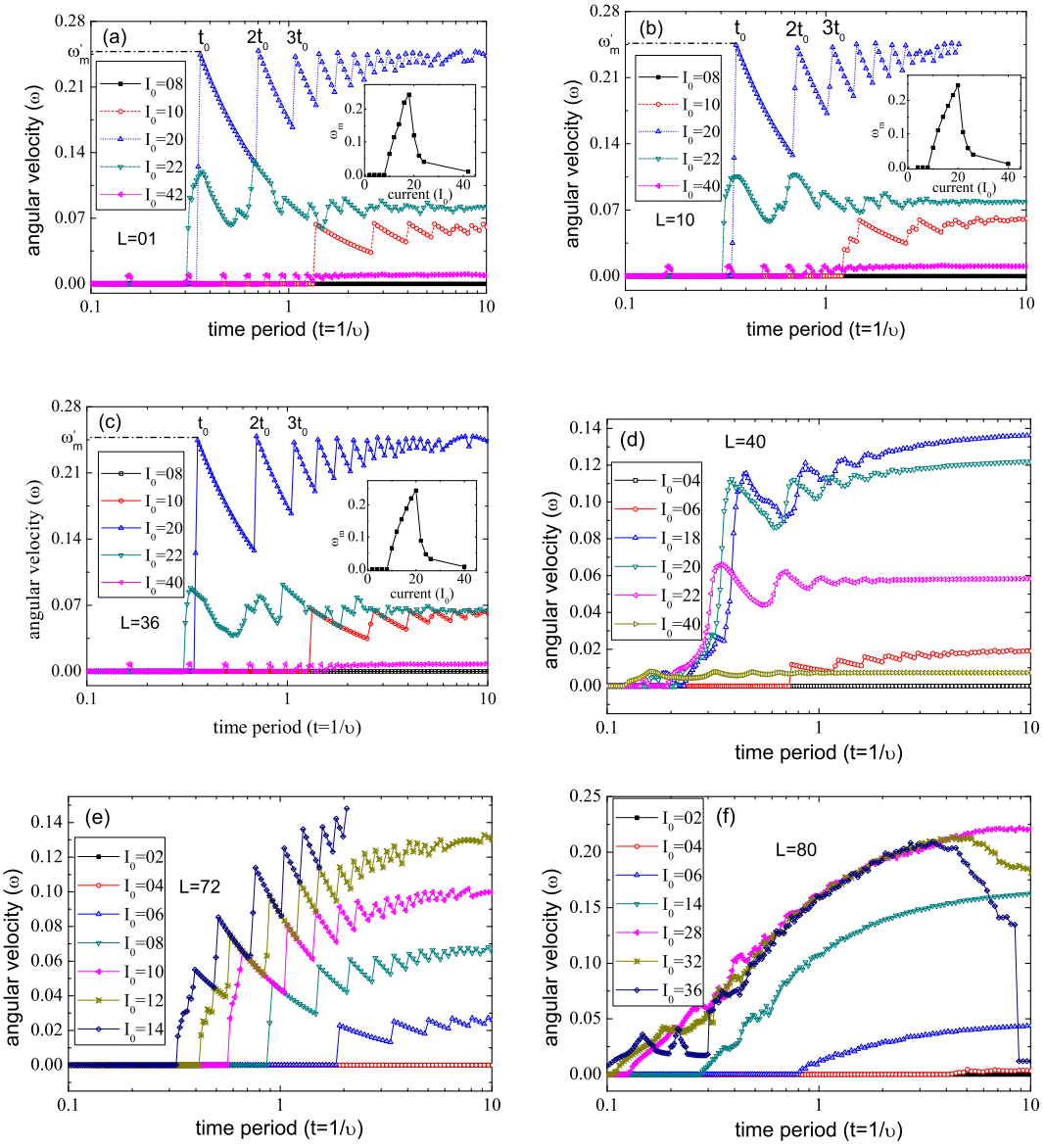

FIG. 10: (Color online) The $\omega - t$ curves in a channel with $g = 0.1$ for different density of vortices: $L/N \ll 1$ (a), $L/N < 1$ (b), $L/N = 1$ (c) (commensurate), $2 > L/N > 1$ (d), $L/N = 2$ (e) (commensurate), and $L/N > 2$ (f). When the density $L/N \leq 1$, i.e., in the single-vortex regime, the angular velocity $\omega(t)$ first reaches the maximum and then oscillates [see (a), (b) and (c)]. With increasing current, the maximum velocity increases until the driving force reaches the value larger than f_m^-. For high density, the angular velocity $\omega(t)$ does not reach the maximum because the vortex motion in the easy direction is compensated by that in the hard direction. $\omega(t)$ increases when the frequency decreases. In commensurate cases [(c) and (e)] $\omega(t)$ oscillates with sharp jumps which are not observed in incommensurate cases for high vortex density (f).

V. EXPERIMENTAL DETECTION OF VORTEX RATCHET EFFECT IN A CORBINO GEOMETRY

To the best of our knowledge, to date there have been no demonstrations of a circular ratchet with vortices in a superconductor. In fact, there are very few experimental examples of ratchets for producing circular motion in any particle system. Thus, to demonstrate the feasibility of the approach employed in our simulations, we have performed preliminary measurements on a device containing a single weak-pinning circular channel for guiding vortex motion in a Corbino geometry. This is based on a technique for using weak-pinning channels with tailored edges to produce asymmetric vortex confining potentials. Such an arrangement resulted in substantial asymmetric vortex response for

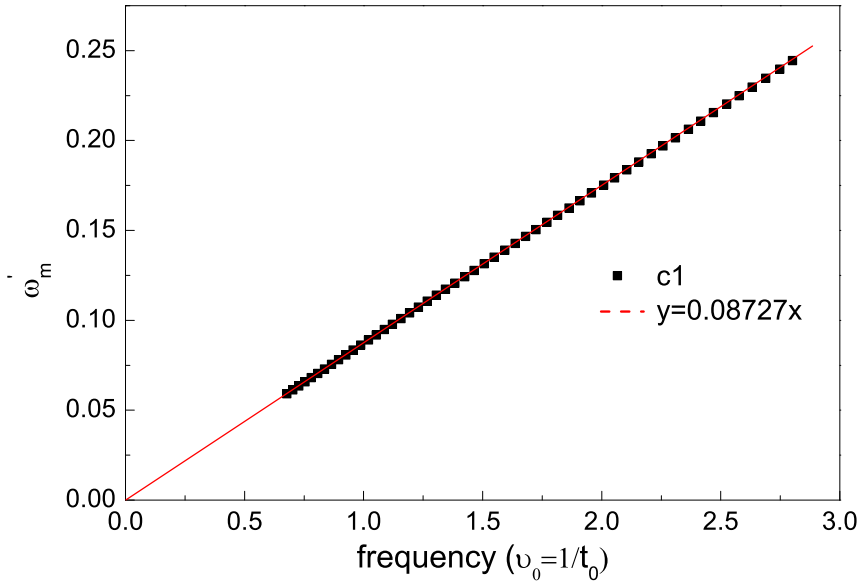

FIG. 11: (Color online) The frequency dependence of the first local maximum ω'_m of the $\omega - t$ curves for vortices in the single-vortex regime when the driving force is smaller than f_m^-. The magnitude of the first peak shows a linear dependence on the principal frequency ν_0.

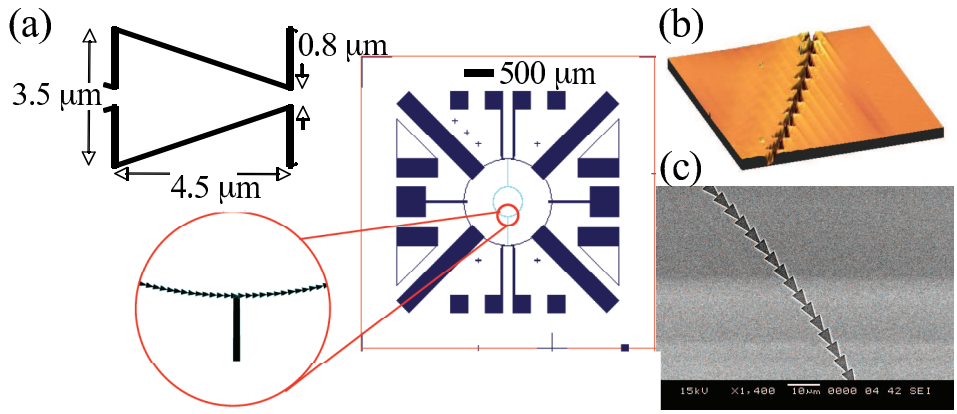

FIG. 12: (Color online) (a) Detail of single ratchet cell of channel and schematic of Corbino ratchet chip layout; extra pads and leads beyond disk were not used for the measurements presented here. (b) Atomic force microscope image of portion of Corbino ratchet channel. (c) Scanning electron micrograph of portion of Corbino ratchet channel.

linear channels on a strip geometry[6]. The Corbino sample consists of a Si substrate with a 200-nm thick film of weak-pinning a-NbGe and a 50-nm thick film of strong-pinning NbN on top. The fabrication followed the scheme of previous weak-pinning channel devices[6,32], with the 1.5-mm diameter Corbino disk pattern etched through the entire superconducting bilayer. The 500-μm diameter circular chain of triangular cells was etched through the NbN layer (Fig. 12), thus defining the weak-pinning a-NbGe channel region for vortex flow.

Wirebonds were attached between the center and perimeter of the Corbino disk for injecting a bias current with a radial flow. Because of the rather small flux-flow voltages for vortex motion in a single channel, it was necessary to use a custom picovoltmeter based on a dc SQUID operated in a flux-locked loop[32]. Measurements of the noise power at different temperatures were used to calibrate the value for the series resistance at the SQUID input, thus allowing for a measurement of the system gain, as described in Ref.[32]. During the measurements, the sample and SQUID were immersed in a pumped liquid helium bath. Shielding of external magnetic fields was achieved with a

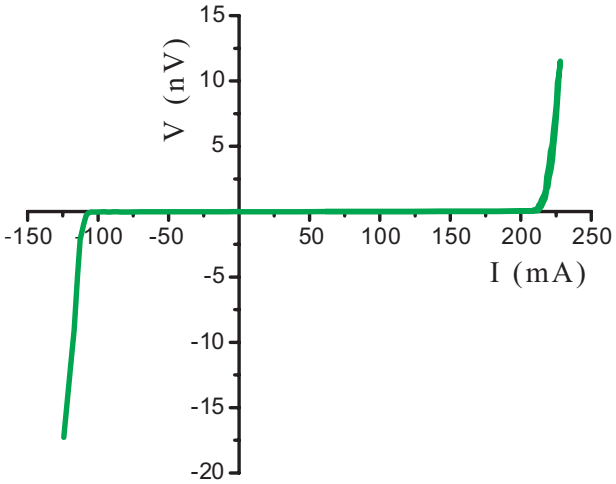

FIG. 13: (Color online) Current-voltage characteristic of Corbino ratchet channel cooled to 1.60 K in an external magnetic field of 0.26 Oe as described in text.

μ-metal shield surrounding the dewar and a superconducting Pb shield around the sample and SQUID on the bottom of the cryogenic insert. Vortices were introduced into the channel by temporarily raising the sample above the helium bath, heating to ∼6 K – between $T_c^{\rm NbGe} = 2.88$ K and $T_c^{\rm NbN} \approx 10$ K – while applying a small magnetic field with a Helmholtz coil on the insert, then cooling back down below $T_c^{\rm NbGe}$.

Upon reaching the desired measurement temperature, the bias current was varied incrementally and the flux-flow voltage sensed by the SQUID was recorded for each current value. Such current-voltage characteristics (IVC) exhibited substantial asymmetries between the critical current for vortices to begin to move through the channel for the two directions. This asymmetry persisted down to the lowest measurement temperature, 1.60 K, well below the onset of superconductivity in the channel at $T_c^{\rm NbGe}$ (Fig. 13). The larger critical current corresponded to the sense of vortex motion in the hard direction through the ratchet cells. Due to experimental wiring limitations on these preliminary measurements of a Corbino ratchet channel, it was not possible to sweep the bias current with an oscillatory drive to study the average flux-flow voltage over a cycle. Nonetheless, the large asymmetry between the two senses of critical current demonstrates the potential for a weak-pinning ratchet channel in a Corbino geometry to rectify vortex motion.

Thus, this provides a motivation for future experiments employing the weak-pinning channel system in a Corbino geometry with a wiring setup optimized for ac driving to explore the various phenomena demonstrated by our simulations.

VI. CONCLUSIONS

A vortex moving in an asymmetric circular channel in a Corbino setup experiences the confinement of the boundary, the repulsive interaction due to other vortices and the gradient (i.e., radially decreasing) driving force when an external current is applied. The combination of these factors determines the vortex motion. Different dynamical behavior is observed in low and high density systems, which are referred to as "single-vortex" and "multi-vortex" regimes, respectively. For low density, i.e., in the single-vortex regime, there is no more than one vortex per triangular cell so that the vortex-vortex interaction is negligible. Therefore, the ratchet potential due to the boundary dominates and all the vortices follow circular 1D trajectories. Since all the vortices still move in 1D when there is more than one vortex per cell (i.e., a higher density), a vortex can escape even easier either in the easy or in the hard direction due to the interaction between vortices in the same cell. This results in decrease of the rectified net current. However, when the number of vortices increases further (i.e., in the"multi-vortex" regime of rectification when the rectified net current increases with the vortex density), the trajectories of vortex motion for low driving currents are 2D while these trajectories squeeze and turn to 1D circle with increasing driving current. Because of the circular geometry of the channel, the density of vortices first becomes inhomogeneous [i.e, see Fig. 5(b)] during the transition from 2D motion to 1D motion in the multi-vortex regime and then becomes homogeneous again when all the vortices move in a circular trajectory.

Considering the asymmetry in the radial direction, vortices near the inner/outer corner of the triangular cells (TCs) (i.e., closer/further to the center of the disk) are driven by different Lorentz forces and for some specific value of driving current the vortex in the outer corner moves to the inner corner while the one in the inner corner moves to the next

TC [e.g., see Fig. 5(a)]. This kind of motion prevents vortices from arriving simultaneously at the narrow part that would lead to jamming which occurs in case of a linear channel. When the density increases, the maximum net angular velocity ω_m remains the same in the single-vortex regime and then decreases until reaching the multi-vortex regime, and then ω_m increases.

The frequency of driving current also strongly influences the vortex dynamical behavior. The ac frequency determines the possible distance a vortex moves during an ac period. For high frequency, a nearly zero net angular velocity is obtained for different values of driving current I_0. Each vortex is unable to overcome the energy barrier and is confined by a single potential well instead of the periodic ratchet potential. When the frequency is low, the ratchet effect is clearly observed in the $\omega - I_0$ curve but the commensurability effect is not present. For an intermediate frequency of driving current under which the distance of moving vortex in a period is comparable to the size of the TC, both the ratchet effect and the commensurability effect have been observed.

Besides the vortex density and the frequency of current, the commensurability between the numbers of vortices and TCs also plays an important role in the dynamical behavior of vortices, which leads to jumps in the angular velocity ω with increasing driving current I_0 (i.e., steps in the $\omega - I_0$ curve). Therefore, under some specific conditions, the average angular velocity of vortices is not a continuous function of the driving current. The commensurability also influences the minimum difference of the angular velocity for different steps in the $\omega - I_0$ curve, and results in integer steps (i.e., the large steps which are found, e.g., for vorticity $L = 1$) and fractional steps (i.e., the smaller steps whose magnitude are fractions of the magnitude of the integer steps, e.g., for vorticity $L = 24$) in a certain range of the current. We also obtained several peaks (sharp jumps) in the $\omega - t$ curve, which correspond to the principal period t_0 (during which the vortex can move over one TC in the easy direction), and harmonics periods $k\nu_0$ ($k = 2, 3, ...$) (during which vortices move over k TCs in the easy direction). The net flow of vortices is enhanced when the ac period is one of the harmonics periods, i.e., the average angular velocity reaches a local maximum.

Acknowledgement

We thank Peter Kes and Marcel Hesselberth for providing the superconducting films from which the Corbino ratchet sample was fabricated. This work was supported by the "Odysseus" Program of the Flemish Government and the Flemish Science Foundation (FWO-Vl), the Interuniversity Attraction Poles (IAP) Programme — Belgian State — Belgian Science Policy, and the FWO-Vl (Belgium). T.W.H., K.Y., and B.L.T.P acknowledge support from the National Science Foundation under Grant DMR-0547147, as well as the use of the Cornell NanoScale Facility, a member of the National Nanotechnology Infrastructure Network, which is supported by the National Science Foundation (Grant ECS-0335765).

[1] E. R. Dufresne, D. Altman, and D. G. Grier, Europhys. Lett. **53**, 264 (2001); E. R. Dufresne, T. M. Squires, M. P. Brenner, and D. G. Grier, Phys. Rev. Lett. **85**, 3317 (2000).
[2] R. D. Astumian, Phys. Rev. Lett. **91**, 118102 (2003).
[3] D.Y. Vodolazov and F.M. Peeters, Phys. Rev. B **72**, 172508 (2005).
[4] S. Savel'ev, V. Misko, F. Marchesoni, and F. Nori, Phys. Rev. B **71**, 214303 (2005).
[5] P. Hänggi and F. Marchesoni, Rev. of Mod. Phys. **81**, 387 (2009).
[6] K. Yu, T.W. Heitmann, C. Song, M. P. DeFeo, B.L.T. Plourde, M.B.S. Hesselberth, and P.H. Kes, Phys. Rev. B **76**, 220507 (2007).
[7] J.F. Wambaugh, C. Reichhardt, C.J. Olson, F. Marchesoni, and F. Nori, Phys. Rev. Lett. **83**, 5106 (1999).
[8] B.L.T. Plourde, IEEE Trans. Appl. Supercon., **19**, 3698 (2009).
[9] C.C. de Souza Silva, J. Van de Vondel, M. Morelle, and V.V. Moshchalkov, Nature **440**, 651-654 (2006).
[10] J.E. Villegas, S. Savel'ev, F. Nori, E.M. Gonzalez, J.V. Anguita, R. García, and J.L. Vicent, Science **302**, 1188 (2003).
[11] J.E. Villegas, E.M. Gonzalez, M.P. Gonzalez, J.V. Anguita, and J.L. Vicent, Phys. Rev. B **71**, 024519 (2005).
[12] J. Van de Vondel, C.C. de Souza Silva, B.Y. Zhu, M. Morelle, and V.V. Moshchalkov, Phys. Rev. Lett. **94**, 057003 (2005).
[13] B.B. Jin, B.Y. Zhu, R. Wördenweber, C.C. de Souza Silva, P.H. Wu, and V.V. Moshchalkov, Phys. Rev. B **81**, 174505 (2010).
[14] R. Wördenweber, P. Dymashevski, and V. R. Misko, Phys. Rev. B **69**, 184504 (2004).
[15] Y. Togawa, K. Harada, T. Akashi, H. Kasai, T. Matsuda, F. Nori, A. Maeda, and A. Tonomura, Phys. Rev. Lett. **95**, 087002 (2005).
[16] C.J. Olson, C. Reichhardt, B. Jankó, and F. Nori, Phys. Rev. Lett. **87**, 177002 (2001).
[17] W. Gillijns, A.V. Silhanek, V.V. Moshchalkov, C.J. Olson Reichhardt, and C. Reichhardt, Phys. Rev. Lett. **99**, 247002 (2007).
[18] P. Hänggi, F. Marchesoni, and F. Nori, Ann. Phys. (Leipz.) **14**, 51-70 (2005).
[19] P. Hänggi and F. Marchesoni, Chaos **15**, 026101 (2005).
[20] D. Cole, S. Bending, S. Savel'ev, A. Grigorenko, T. Tamegai, and F. Nori, Nature Materials **5**, 305-311 (2006).
[21] C. Reichhardt, C.J. Olson, and F. Nori, Phys. Rev. Lett. **78**, 2648 (1997); Phys. Rev. B **57**, 7937 (1998); Phys. Rev. B **58**, 6534 (1998).
[22] V.R. Misko, S. Savel'ev, A.L. Rakhmanov, and F. Nori, Phys. Rev. Lett. **96**, 127004 (2006); Phys. Rev. B **75**, 024509 (2007).
[23] C.J. Olson Reichhardt and C. Reichhardt, Phys. Rev. B **81**, 224516 (2010).
[24] C. Reichhardt and C.J. Olson Reichhardt, Physica C **470**, 722 (2010).
[25] Q. Lu, C.J. Olson Reichhardt, and C. Reichhardt, Phys. Rev. B **75**, 054502 (2007).
[26] C.S. Lee, B. Jankó, I. Derényi, and A.L. Barabási, Nature **400**, 337-340 (1999).
[27] K. Yu, M.B.S. Hesselberth, P.H. Kes, and B.L.T. Plourde, Phys. Rev. B **81**, 184503 (2010).
[28] C. Reichhardt and C.J. Oslon Reichhardt, Phys. Rev. E **68**, 046102 (2003).
[29] C.J. Oslon Reichhardt and C. Reichhardt, Physica C **432**, 125 (2005).
[30] E.M. Gonzalez, N.O. Nunez, J.V. Anguita, and J.L. Vicent, Appl. Phys. Lett. **91**, 062505 (2007).
[31] A.V. Silhanek, J. Van de Vondel, V.V. Moshchalkov, A. Leo, V. Metlushko, B. Ilic, V. R. Misko, and F. M. Peeters, Appl. Phys. Lett. **92**, 176101 (2008).
[32] T.W. Heitmann, K. Yu, C. Song, M.P. DeFeo, B.L.T. Plourde, M.B.S. Hesselberth, and P.H. Kes, Rev. Sci. Instrum. **79**, 103906 (2008).
[33] D. López, W. K. Kwok, H. Safar, R.J. Olsson, A. M. Petrean, L. Paulius, and G. W. Crabtree, Phys. Rev. Lett. **82**, 1277 (1999).
[34] G. W. Crabtree, D. López, W. K. Kwok, H. Safar, and L. M. Paulius, J. Low Temp. Phys. **117**, 1313 (1999).
[35] M. C. Miguel and S. Zapperi, Nature Materials **2**, 477 (2003).
[36] P. Benetatos and M. C. Marchetti, Phys. Rev. B **65**, 134517 (2002).
[37] V. R. Misko and F. M. Peeters, Phys. Rev. B **74**, 174507 (2006).
[38] N. S. Lin, V. R. Misko, and F. M. Peeters, Phys. Rev. Lett. **102**, 197003 (2009); Phys. Rev. B **81**, 134504 (2010); V. R. Misko, N. S. Lin, and F. M. Peeters, Physica C **47**, 939 (2010).
[39] M.C. Miguel, A. Mughal, and S. Zapperi, Phys. Rev. Lett. **106**, 245501 (2011).
[40] S. Okuma, Y. Tsugawa, and A. Motohashi, Phys. Rev. B **83**, 012503 (2011).
[41] B.J. Baelus, L.R.E. Cabral, and F.M. Peeters, Phys. Rev. B **69**, 064506 (2004).
[42] I.V. Grigorieva, W. Escoffier, V.R. Misko, B.J. Baelus, F.M. Peeters, L.Y. Vinnikov, and S.V. Dubonos, Phys. Rev. Lett. **99**, 147003 (2007).
[43] D. Babic, J. Bentner, C. Surgers, C. Strunk, Phys. Rev. B **69**, 092510 (2004).
[44] A.I. Larkin and Y.N. Ovchinnikov, Zh. Eksp. Teor. Fiz. **68**, 1915 (1975).
[45] W. Klein, R.P. Huebener, S. Gauss, J. Parisi, J. Low Temp. Phys. **61**, 413 (1985).